Chapter 4

Ultrathin oxides: representative surface models or unique films?

4.1 Introduction

In this Section we will discuss how thin oxide films compare to the corresponding bulk materials and their surfaces. We will approach this question from a ground-state perspective and employ density-functional theory for this purpose. As already mentioned in the introductory Chapter, we will focus mainly on the implications for heterogeneous model catalysts, in which ultrathin oxide films of often only one or two monolayers (ML) thickness are used to represent an oxide support material of macroscopic thickness. This is a drastic approximation and requires a systematic investigation of the relevant aspects to learn more about the significance of surface science experiments for the situation on a real oxide surface.

In order to analyse the differences between an ultrathin oxide film on a metal substrate and the surface of a bulk oxide, it is helpful to consider intermediate steps between the two limiting cases. We have sketched such a "pathway" in Fig. 4.1 where we take apart the supported thin film system in a controlled manner and "transform" it into the surface of a bulk oxide. In contrast to experiment, this is easily achieved in theory and helps to disentangle the mutual influence of the substrate/film interface, the unique atomic configurations within the thin film, and the evolution of a bulk-like behaviour when going from a two-dimensional film to a three-dimensional bulk system. First we ask the question what role the substrate plays for the properties of the thin film. When the supported film is linked to the metal substrate

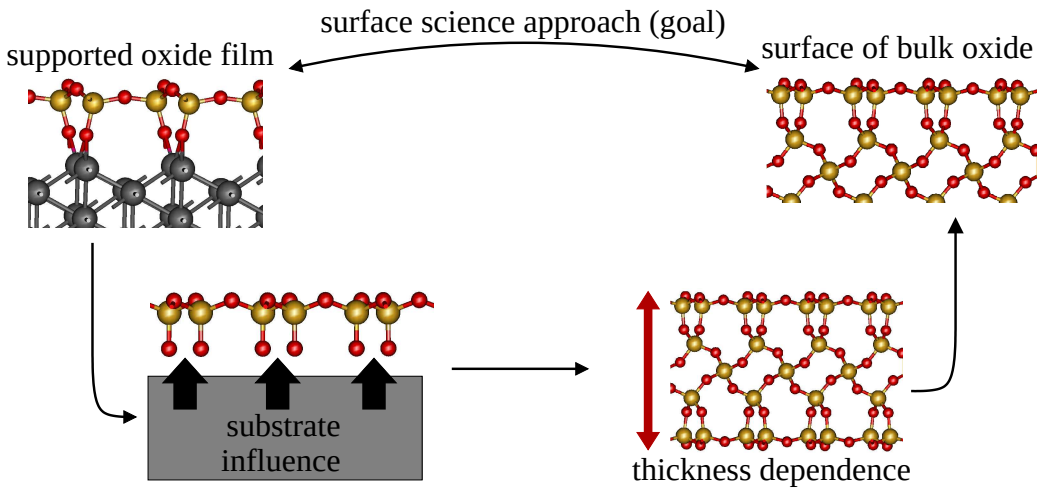

Figure 4.1: Important aspects of the comparison between supported thin films and bulk surfaces.

by strong chemical bonds (which is the case for e.g. silica and alumina), this implies a strong influence of the interface on the local bonding arrangements. Moreover, the surface lattice constants of commensurate well-ordered films are determined by the lattice constant of the respective substrate.[1] In Section 4.3, we will study the substrate influence for the example of the thin silica film on Mo(112) since this film fortuitously resembles an α-quartz (0001) surface and is hence not specific to the Mo(112) substrate.

The thickness of the film is the second key aspect and will be the topic of Section 4.4. It is well known that the properties of nanosized materials may differ significantly from their bulk counterparts, to which various factors contribute. For instance, films that are only a few atomic layers thick expose a significant part of their atoms at the surface. The surface may then influence or even dominate the properties of the film. Furthermore, the charge separation to form ions and hence the ionic bonding is a cooperative effect: the local charge transfer from a cation to an anion is enhanced by the Madelung field of the surrounding ions, which in turn depends on the charge of these ions. In a film of finite thickness, this cooperativity is disturbed.

[1] We note here that this provides a simple explanation for the structural wealth of the thin silica and alumina films. The bulk oxide structure does usually not match well with the substrate and would experience considerable strain, even when taking into account that the optimized lattice constant for a (freestanding) thin film may in general deviate from its bulk value [91]. This strain can be released either by the introduction of lattice defects – up to the point where the film becomes essentially amorphous – or by reconstructions at specific thicknesses. This point will be addressed in more detail in Sec. 4.3.4.

For ultrathin films also quantisation and confinement effects should be considered. They usually become important when the thickness of the film falls short of the typical length scale of the electron or hole states, but our studies show that they play no important role for the oxides studied in this work. To ensure that the chosen films systematically converge towards the bulk we study these effects for free-standing films in a surface unit cell compatible to the bulk. The thickest films then correspond to the slab models routinely used to model surfaces in theoretical simulations. The goal of studying the thickness dependence with free-standing films without a substrate is not to judge the suitability of a particular film for a particular purpose, but serves mainly to identify general systematic trends. We therefore consider three characteristic oxides (silica, alumina, and hafnia) not only from the field of heterogeneous catalysis, but also for electronic device applications where the possible thickness dependence may set a limit in the on-going trend to smaller and smaller devices. Silica and alumina are important support materials for noble-metal catalysts. All three oxides are current materials for the insulating layer in field-effect transistors, which are the heart of every modern integrated circuit, and we thereby touch another area in which the properties of ultrathin oxide films are of great interest.

For both steps of our pathway, we will focus the comparison on the differences in the atomic and electronic structure, which are the key properties to which many others such as the chemical, spectroscopic, or dielectric properties are correlated. The atomic structure is well described with DFT-LDA. We will assess the changes in the electronic structure from a ground-state perspective, too. The DFT-LDA density of states (DOS) reflects the influence of several relevant physical effects, such as quantum confinement, the electrostatic potential, or the hybridisation of different atomic states, but may not directly be compared to experiments which probe the quasiparticle spectrum such as photoelectron spectroscopy. For a direct comparison with these techniques, quasiparticle corrections must be included. This will be discussed in Chapter 5, where we will show for a computationally feasible system that the quasiparticle spectra of supported insulator films will include additional image potential effects absent from the DFT-LDA ground-state calculations. However, we will show here in Sec. 4.3.3 that the DFT-LDA electronic structure is sufficient to qualitatively explain several aspects of the experimental spectra from ultraviolet photoelectron spectroscopy (UPS) and metastable impact electron spectroscopy (MIES).

The physical and chemical principles that govern the ionic bonding in the bulk materials apply to the thin films, too. It is therefore instructive to recapitulate the properties of the bulk materials, which will be done in Section 4.2.

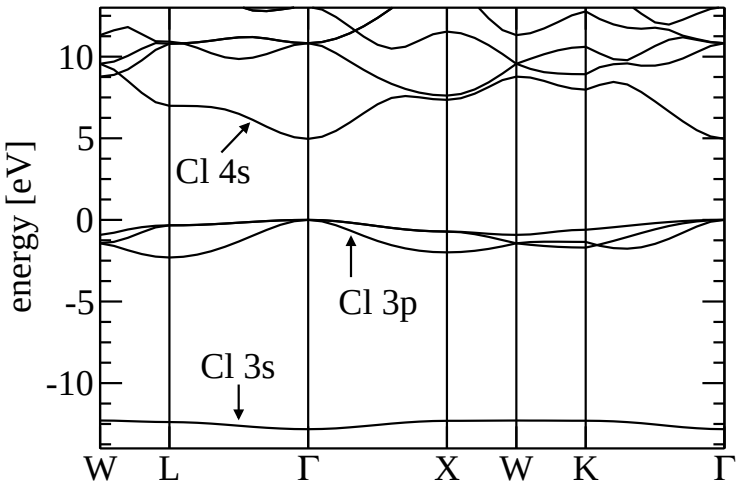

Figure 4.2: DFT-LDA band structure of bulk NaCl at the theoretical lattice constant (5.49 Å).

4.2 Properties of the bulk materials

In this Section we will briefly summarise the atomic and electronic structure of the bulk materials from which the thin films in this work are derived. In addition to the oxides that are the subject of this Section (silica, alumina, and hafnia) we will also include sodium chloride here since it exemplarily demonstrates the characteristic properties of wide-gap insulators and will be used to investigate G_0W_0 effects in Chapter 5.

4.2.1 Sodium chloride

Sodium chloride is probably *the* prototypical ionic material. It crystallises in the rocksalt structure, where each ion is octahedrally surrounded by six ions of opposite charge. The experimental lattice constant is 5.63 Å, compared to our theoretical equilibrium constant at the DFT-LDA level of 5.49 Åwhich agrees with all-electron results. We attribute this underestimation by about 3% mainly to the description of exchange and correlation between the Na^+ core and the valence electrons in the LDA. Also metallic sodium (which consists of Na^+ and an essentially homogeneous electron gas) shows a similar underestimation of the lattice constant [92]. This is further corroborated by the comparison to a GGA functional (PBE in this case) for the Na^+ ion: while the density is almost indistinguishable from the LDA, the effective potential is noticeably less attractive in the GGA than in the LDA. Indeed, the GGA functionals give significantly improved lattice constants for metallic sodium

[92].

The electronic structure is simple, cf. Fig. 4.2. In the following bulk band structures, the valence band maximum defines the energy zero. We will focus on the DFT-LDA electronic structure at the theoretical lattice constant in the following. Applying G_0W_0 corrections mainly affects the gaps between the bands[2] while leaving the band dispersion essentially unchanged. The valence part of the bandstructure consist of two bands, a 0.5 eV wide band with mainly Cl 3s character and a 2.3 eV wide band dominated by the Cl 3p orbitals with some admixture of Na 3s and 3p states. Using the atomic orbital (AO) projection technique described in App. D.1, we finde that the Na-centered orbitals contribute, depending on the **k**-point, only 0–12 % to the norm in the AO basis for these states, whereas the Cl orbitals account for 85–99%. The lowest conduction band begins 5.0 eV above the valence band maximum (DFT-LDA). Its character is more difficult to assess since different approaches give different results. A detailed discussion is given in Sec. D.2. In brief, we find that it is a hybridisation of the Na 3s and 3p states with a chlorine scattering state (which may be denoted Cl 4s). The chlorine 4s plays a crucial role for the dispersion of this band, while its energetic position is determined by the sodium states.

A highly dispersive conduction band similar to the one discussed here is found in all binary main group compounds that are ionic insulators, for instance the alkali halides and earth-alkali chalkogenides. Notably, the wide-gap oxides considered next all show such a O 3s-derived, free-electron-like band, which hybridises with the cation states to a lesser extent than what we observe for the conduction band in NaCl. The valence part of the oxides is – as in NaCl – dominated by the anion states (i.e. O 2p) with a few percent admixture of the cation states. We will now proceed to the discussion of the individual oxides.

4.2.2 α-Quartz

Our first example will be silica, or silicon dioxide (SiO_2). Silica has a large number of polymorphs. The ratio of the tabulated ionic radii [94] of Si^{4+} (0.54 Å) and O^{2-} (1.26 Å) is 0.429, very close to the critical value for octahedral coordination (0.414, [94]). Most polymorphs therefore assume a tetrahedral coordination for the silicon centres and a two-fold coordination for the oxygen, often denoted as 4:2 coordination. Only the metastable stishovite

[2]The conduction band is shifted upward by 3.3 eV relative to the valence band maximum. The quasiparticle gap then becomes 8.3 eV in reasonable agreement with experiment (8.5 eV [93]). The Cl 3s band is shifted upward by 0.5 eV. We also find that the G_0W_0 corrections change only negligibly when the lattice constant is varied by a few percent.

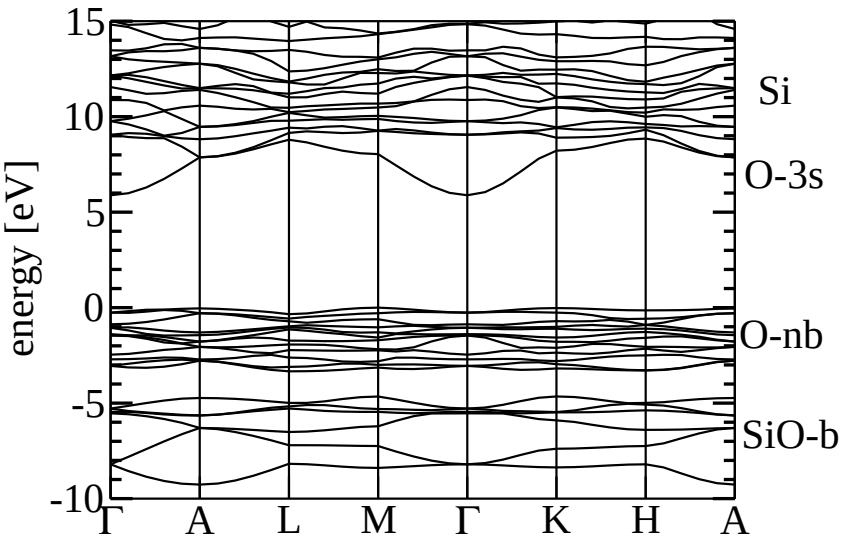

Figure 4.3: DFT-LDA band structure of bulk α-quartz.

phase with a rutile structure shows a octahedral 6:3 coordination. In the tetrahedral phases, the Si-O bond length is $\sim$1.6 Å and the Si-O-Si angle varies between $\sim$140° and 180° [95]. The bond length is shorter than the empirical estimates for a purely ionic bond (1.80 Å) and lies between the values for a covalent single bond (1.77 Å) and a double bond (1.53 Å). A considerable covalent character has therefore been ascribed to the chemical bonds in SiO_2. The structure of the 4:2-coordinated phases can be characterised as a network of $[SiO_4]$ tetrahedra connected at their corners. The polymorphs then differ in the long-range order of the $[SiO_4]$ units. Correspondingly, their energetic stability is very similar [95]. The most stable silica polymorph is α-quartz, where the tetrahedra form interconnected helical chains.

The electronic band structure of α-quartz is shown in Fig. 4.3 and can be understood as follows: The occupied states are derived from oxygen $2p$ orbitals with some admixture of the Si $3s$ and $3p$ states. Since oxygen is only two-fold coordinated, the O $2p$ orbitals split into two subbands: those that point towards the Si neighbours form the Si-O bonding (SiO-b) bands have some Si character. The other two orbitals form very flat, oxygen non-bonding (O-nb) bands, which are separated from the SiO-b subband by a gap of $\sim$1 eV. This separation into SiO-b and O-nb subbands exists for all 4:2-coordinated silica bulk phases. The lowest conduction band is the O-$3s$ band hybridising to some extent with Si states. Most of the very flat bands at higher energies derive from Si. At the optimised lattice constant, we find

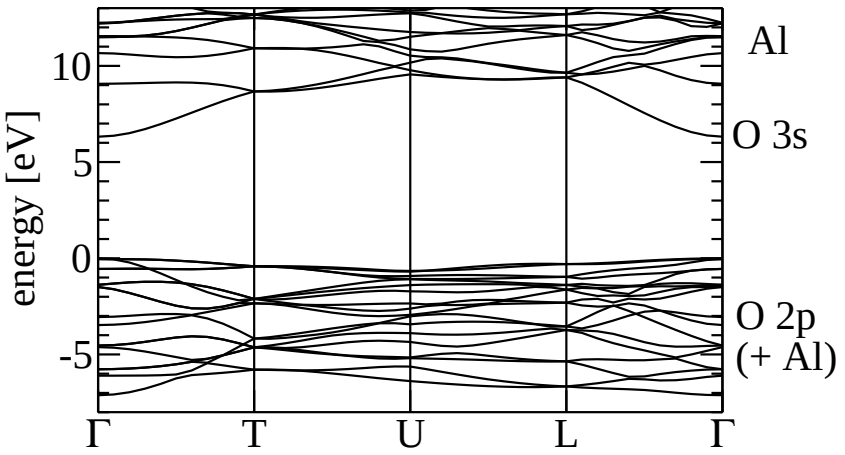

Figure 4.4: DFT-LDA band structure of bulk α-alumina

an indirect band gap of 5.9 eV between M[3] and Γ (DFT-LDA). The total O-2p band width is about 9.3 eV.

4.2.3 α-Alumina

The second oxide that we will consider is alumina. Other than silica, its structure is easily understood from close-packing arguments. In accordance with the ratio of the ionic radii (0.68 Å:1.24 Å=0.55, [94]), the aluminium ions in α-alumina, or corundum, have an octahedral coordination. The oxide ions form a close-packed hexagonal structure and are surrounded tetrahedrally by Al. α-alumina is the thermodynamically most stable phase at ambient conditions. A second polymorph, γ-alumina, is a high-temperature phase with a lower density than α-alumina. In γ-alumina, the oxide ions form a close-packed cubic structure, where the aluminium ions statistically occupy both tetrahedral and octahedral sites [94]. We point out that the lower density in γ-alumina is accompagnied by a lower average coordination of the aluminium atoms, a motif that plays a role also for supported thin films. Since many alumina thin films exhibit Al ions in tetrahedral configurations, too, they are often classified as γ-like (e.g. on $Ni_3Al(111)$ [96], NiAl(001) [97], or NiAl(110) [98]). However, the lack of long-range order makes γ-alumina unsuitable for our theoretical investigations. We therefore focused our investigations on α-alumina.

The band structure of α-alumina is presented in Fig. 4.4. The oxygen 2p-orbitals form the valence band with a width of 7.1 eV, somewhat smaller

[3]However, the valence band at K is only 0.02 eV lower

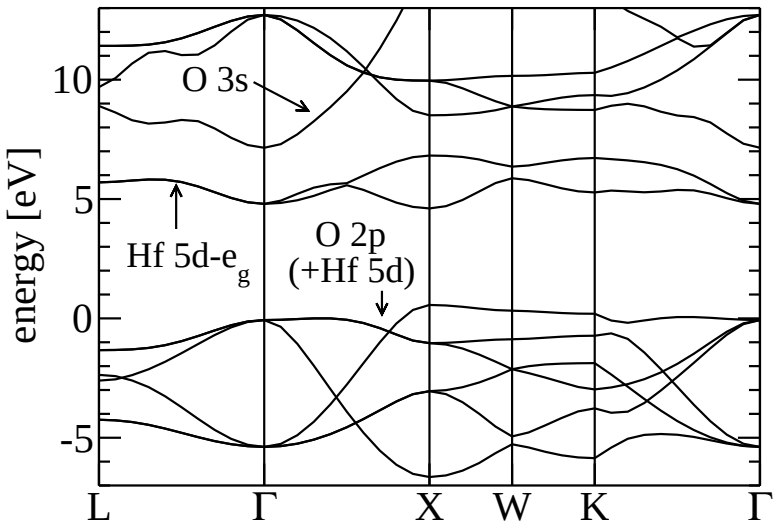

Figure 4.5: DFT-LDA band structure of bulk cubic hafnia

than in α-quartz. A separate oxygen non-bonding subband like in silica does not exist due to the tetrahedral configuration of the oxide ions. The band gap is direct at Γ and amounts to 6.3 eV (DFT-LDA), similar to the direct band gap in α-quartz (6.1 eV). As in silica, the lowest conduction band has a very strong oxygen 3*s* character with some admixture of Al 3*s*.

4.2.4 Cubic hafnia

Hafnium has the largest cation of the three oxides considered (ionic radius ratio 0.97 Å:1.24 Å=0.78), which makes a cubic coordination of the hafnium ions possible. The stable bulk form at room temperature is monoclinic hafnia with a 7-fold coordination. However, we focus on the high-temperature polymorph cubic hafnia here because it appears to play an important role in hafnia thin films [99, 100]. It has a CaF_2 structure with 8-fold cubic coordination of the hafnium ions, and correspondingly a tetrahedral configuration for the oxygen atoms.

The electronic structure of hafnia (see Fig. 4.5) shows a stronger influence of the metal than silica or alumina. The upper valence band has metal-oxygen bonding character and is 7.2 eV wide, similar to the band width in alumina (7.1 eV) which has the same oxygen coordination. The band gap (direct at X) is 4.0 eV (DFT-LDA)[4]. The conduction band derives from the Hf-5*d* states, which are split by the cubic crystal field into t_{2g} and e_g states. The

[4]Experimental data is not available since the bulk cubic hafnia is not stable at room temperature

latter form the bottom of the conduction band. A band with mainly O-3s character can be identified close to the Γ point at about 7.2 eV above the top of the valence band. At other **k**-points, it hybridises with the t_{2g} states.

4.2.5 Comparison of the oxides

Having presented the different bulk materials, we will now discuss how the ionic properties may be modified in a thin film. For this purpose let us imagine the (hypothetical) case of forming a film directly from the bulk material. To achieve this, several ionic bonds have to be broken. Since the ionic bonds are not directed, the ions rearrange to either increase their coordination or to reduce the repulsive interactions between the ions of equal charge, thereby increasing the local symmetry of the coordination shell. The magnitude of these relaxations or reconstructions depends on the relative number of broken bonds. Therefore, the small coordination numbers in silica will lead to significant reconstructions because already a single broken bond represents a large disturbance. For cubic hafnia, on the other hand, reconstructions are unlikely to occur (and indeed not observed for other examples of this structure type such as CaF_2 and CeO_2) because most of the bulk environment is still present, and also the relaxations are small (see Sec. 4.4.3). A second important point is the density of the bulk structure, since it is connected to the flexibility of the oxide. Very open structures like that of silica undergo reconstructions involving several layers. In alumina, the close-packed oxide layers tolerate only minor changes within the layers and only the inter-layer separation is a flexible degree of freedom.

What can we then expect for the electronic structure? The bulk bands of all three oxides are very similar in their character, width, and also the gaps between them. Characteristic are the localised O 2p states[5], forming a 7–9 eV wide valence band, and a dispersive O 3s band in the conduction band starting 6–7 eV above the top of the valence band. Only in hafnia, additional metal states appear between these oxygen-derived states. The localised states will not be affected strongly by perturbations in the long-range order, but change sensitively when the local order is modified. The formation of a thin film can be seen as a perturbation of the long-range order. If the most of the atoms thereby remain in a bulk-like local environment, the overall features of the electronic structure of a thin film are therefore expected to be similar to those of the bulk oxide. On the other hand, changes in the local coordination shell due to the subsequent relaxation are very important for the details of the electronic structure.

[5]Localisation here refers to the extent of the atomic orbitals contributing to a band.

4.3 Substrate influence for silica films

In this Section we will investigate how a metal substrate influences and modifies the properties of a thin film for a specific example: silica on Mo(112). The system represents an experimental breakthrough in the growth of crystalline silica films. While silica films on Mo(100) and Mo(110) are amorphous [101–103], the silica film on Mo(112) shows a very sharp c(2×2) LEED pattern. It has been studied with a variety of experimental techniques, including low-energy electron diffraction (LEED) [16, 17, 104–106], Auger electron spectroscopy (AES) [16, 17, 104, 105], X-ray photoemission spectroscopy (XPS) [104, 105], ultraviolet photoemission spectroscopy (UPS) [17, 106], metastable impact electron spectroscopy (MIES) [17], IRAS (infrared reflection absorption spectroscopy) [17, 106], high resolution electron energy loss spectroscopy (HREELS) [13, 16], and scanning tunneling microscopy (STM) [13, 106]. The structure of this film has been a matter of debate [16, 104–107] that has been recently solved by means of DFT calculations [13, 14]. We will first show that the structure of the well-ordered silica film on Mo(112) is closely related to the reconstructed α-quartz (0001) surface. This fortuitous similarity motivated us to study the influence of the substrate for this system, while for instance alumina films usually strongly deviate from any known alumina surface. We employ DFT to compare the atomic and electronic structure between the silica film on Mo(112) and the α-quartz (0001) surface. The key aspects of the substrate influence identified here are are then later used to discuss other oxide films. We will also compare our computed electronic structure to UPS and MIES experiments for the silica film on Mo, demonstrating that the observed features are characteristic for the SiO_2/Mo(112) system, but not for silica surfaces. Finally we will draw some conclusions on the use of supported monolayer-thin films in heterogeneous catalyst studies.

4.3.1 Atomic structure: the siloxane surface

A reliable atomistic model of the thin silica film on Mo(112) has only recently been found by a combination of DFT simulations and several experimental techniques, including STM, XPS, and HREELS [13, 14, 108]. The local atomic structure of the film corresponds to that of the tetrahedral silica polymorphs, but its long-range order is notably different. The [SiO_4] tetrahedra form a two-dimensional, perfectly bonded hexagonal network, which is linked to the substrate via oxygen atoms (cf. Fig. 4.6). The film is one monolayer thick, and it is not possible to add further silica layers without destroying the surface. This warrants the conclusion that the film corresponds to a surface

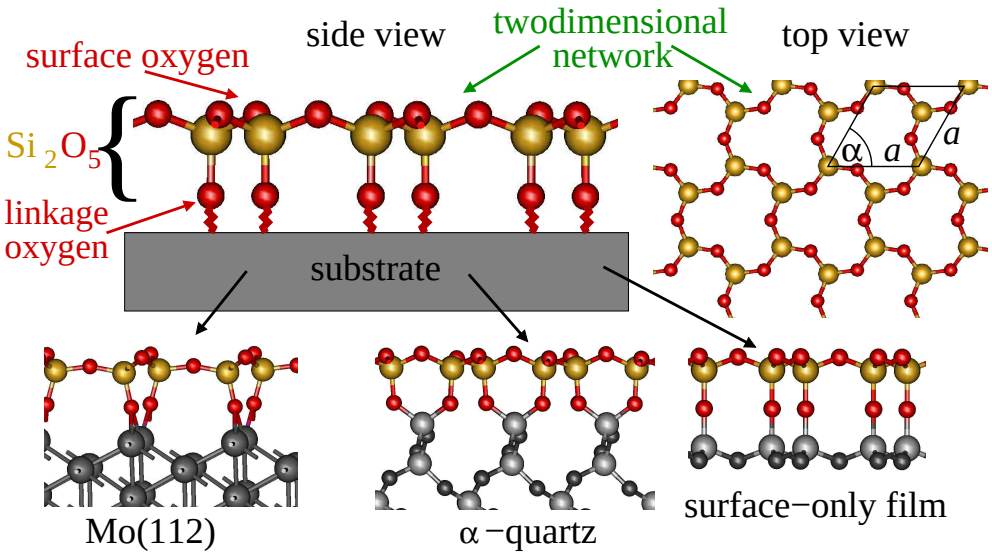

Figure 4.6: Structure of the siloxane surface on Mo(112), α-quartz, and the hypothetical freestanding surface-only film. Red spheres indicate oxygen atoms, yellow spheres silicon atoms.

form of silica. A comparison to known silica surface and thin film structures reveals that the bonding pattern, i.e. the connectivity and long-range order of the [SiO_4] units, is identical to the "dense" reconstruction of the α-quartz (0001) surface [109], the "silicate adlayer" on 4H and 6H SiC [110], and the "siloxane surface" of clay minerals [111]. In the following, we will refer to this surface form as "siloxane surface" because it emphasises the "siloxane bond" Si-O-Si as characteristic surface motif as opposed to hydroxyl groups or unsaturated bonds.

Having established the similarity between the silica film on Mo(112) and the α-quartz(0001) surface, we will now compare the atomic structure in detail. The main question we pose is how well the silica film found in experiment represents the corresponding α-quartz surface. To our knowledge a well-ordered, dry α-quartz surface has not yet been observed in experiment, where amorphous and partially hydroxylated surfaces prevail. However, theoretical simulations predict it to be the most stable surface structure in the absence of hydrogen [109] in full agreement with our own results (see Sec. C.1). We will denote the two systems as the siloxane surface on a Mo and on a quartz substrate, respectively. As starting point for the structure optimisation of the c(2×2) silica film on Mo(112) in our DFT-LDA calculation, we assume the most stable configuration identified by Todorova *et al.* [13, 108], where the linkage oxygens occupy a two-fold bridge position on the Mo rows of the

	Mo(112)	α-quartz(0001)	Si_4O_8
a [Å]	5.21 (5.22)	4.85 (4.92)	5.24
α [°]	63	60	60
area [Å^2]	24.2 (24.3)	20.4 (21.0)	23.8
Si-O (surface) [Å]	1.61–1.63	1.60–1.61	1.61
Si-O (bridge) [Å]	1.63	1.62–1.63	1.61
Si-O-Si (surface) [°]	134, 162	118–125	141
[SiO_4] rotation [°]	0.1-0.2	21-22	0
[SiO_4] tilting [°]	14	4	0
O buckling [Å]	0.4	0.2	0

Table 4.1: Structural parameters (DFT-LDA) of the siloxane surface on Mo(112) and α-quartz and the relaxed pure-surface Si_4O_8 model in comparison. Numbers in brackets refer to experimental data.

(112) surface. The small differences in the structural parameters reported here and in [13] can be traced to the different functional (GGA) employed and reflect the well-known trends towards larger bond lengths in the GGA. The Mo substrate is modelled by 5 layers[6] and the surface unit cell corresponds to a c(2×2) superlattice of the (112) surface of Mo at the theoretical bulk lattice constant (3.139 Å). The α-quartz (0001) surface is modelled by a symmetric Si_8O_{16} slab at the theoretical lattice constant of α-quartz. To learn more about the intrinsic structural properties of the "ideal" siloxane surface when the lattice constant is varied, we have additionally studied a pure-surface Si_4O_8 film (cf. Fig. 4.6).

The structural parameters of the siloxane surface for the three cases are summarised in Tab. 4.1. As we will show in the following, the influence of the substrate on the structure of the siloxane surface can be attributed to two key factors: the lattice constant of the substrate and the linkage of the film to the surface of the substrate. The siloxane surface adapts to these constraints easily by reorienting the tetrahedral building blocks, a relaxation mode that mostly affects the rather flexible Si-O-Si angles. The harder degrees of freedom such as the Si-O bond length remain almost identical to those of bulk α-quartz (cf. Tab. 4.1).

Let us focus on the role of the lattice constant first. The structural properties of an "ideal" siloxane surface independent of its substrate were studied with the free-standing Si_4O_8 film that consists of two siloxane-surfaces directly linked together. When the lattice constant of this film is varied, the behaviour below and above the optimum lattice constant of 5.24 Å differs (cf.

[6]Using 7 Mo layers shows negligible differences.

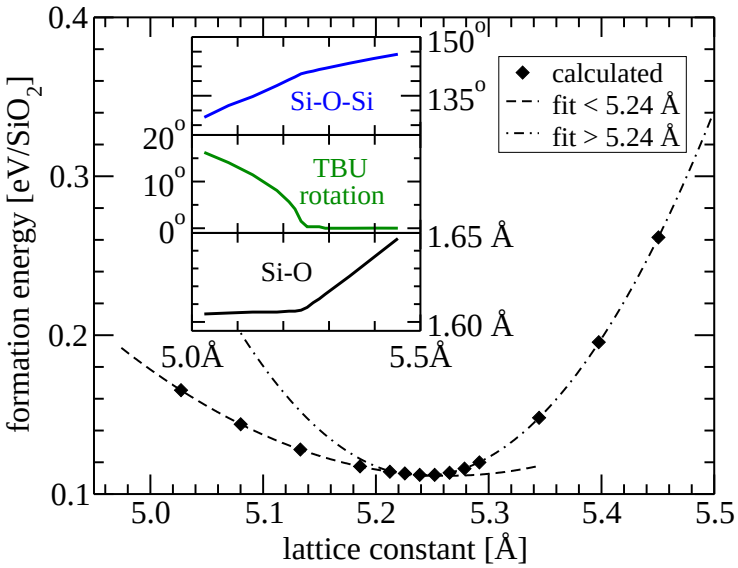

Figure 4.7: Formation energy and important structural parameters as a function of the lattice constant for the siloxane pure-surface Si_4O_8 film. To demonstrate the different behaviour above and below 5.24 Å, separate quadratic functions have been fitted to the two regions.

Fig 4.7). The formation energy on either side of the minimum is a quadratic function of the lattice constant, but the curvature differs by a factor of ∼3. Under compression, the energy rises more slowly since the surface network adapts by rotating the [SiO_4] tetrahedra along their vertical axis, a very soft degree of freedom. We use the in-plane component of the Si-Si-O angle to monitor this rotation (schematically illustrated in Fig. 4.8 a). This rotation mechanism is known from phyllosilicates [112] and results in a reduction of the Si-Si distance (and hence the lattice constant) with only moderate changes at the oxygen atoms. At the energy minimum, the rotation angle has reached zero. Under further expansion, the [SiO_4] tetrahedra are distorted and the Si-O bonds are stretched. Since harder degrees of freedom are involved in this case, the energy rises more quickly than under compression. The relaxation of the siloxane surface on the Mo and α-quartz substrates follows the same pattern. The lattice constant of the quasi-hexagonal c(2×2) Mo(112) superlattice (a=5.21 Å and α=63°) is very close to that of the "surface-only" Si_4O_8 film (5.24 Å). Correspondingly, the [SiO_4] rotation about the surface normal is essentially zero. We note that the lattice constant of the ($\sqrt{3}\times\sqrt{3}$)R30° pattern observed for the SiC substrates [110] is 5.25 Å (DFT-LDA [113]) and matches very well with the relaxed surface, too. This provides a simple explanation why the siloxane surface forms readily on

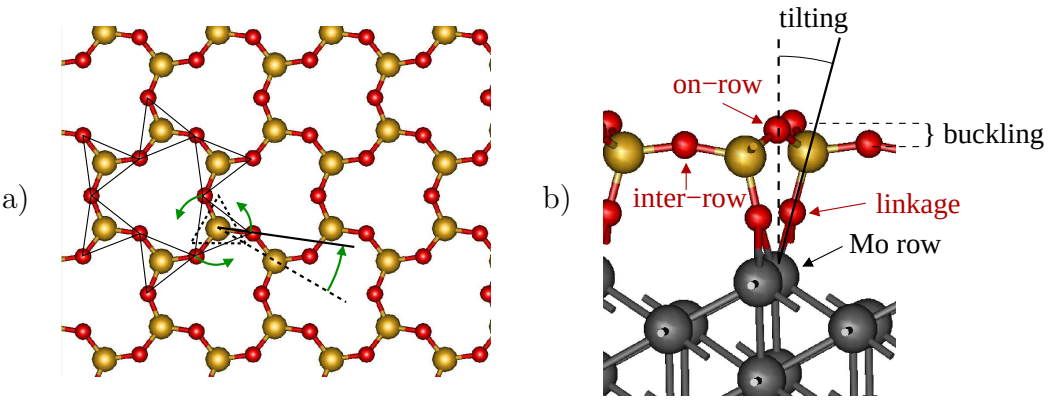

Figure 4.8: a) [SiO_4] rotation, schematically. b) Definition of tilting and buckling for the siloxane surface.

the lattice-matched substrates Mo(112) and 4H/6H-SiC (0001). The lattice match is of course only one of several factors determining the stability. The linkage to the substrate is another one as discussed below for Mo(112). In the case of SiC, this is almost ideal (hexagonal pattern of dangling Si bonds). The lattice mismatch to α-quartz (4.85 Å) on the other hand amounts to 8%. As in the pure-surface model, the compression of the siloxane surface on the quartz substrate is accompanied by a large [SiO_4] rotation ($\sim$20°). The considerable lattice mismatch probably introduces a significant number of defects in real α-quartz surfaces and explains the lack of long-range order. The defects may then be responsible for its propensity towards hydroxylation.

Apart from the lattice constant, the oxygen linkage to the substrate is an important factor, too. The Mo(112) surface exhibits rows to which the linkage oxygen atoms bind in a two-fold bridge position [13]. The three surface oxygen atoms of the two-dimensional network thus become nonequivalent: two of them link [SiO_4] units along the same row and one forms the inter-row connections (cf. Fig. 4.8 b). In order to achieve the bonding to the substrate, the trifold symmetry axis of the [SiO_4] tetrahedra is tilted by 14° against the surface normal towards the inter-row oxygen. The bonding angle at this atom (162°) is considerably larger than along the row (134°). The tilting also introduces a height difference (buckling, cf. Fig. 4.8 b) for the surface atoms of $\sim$0.4 Å. The siloxane surface on quartz, however, tilts only by 4° and buckles by 0.2 Å. The tilting and buckling on α-quartz are smaller because not only the bulk-truncated quartz substrate matches better with the preferred hexagonal arrangement of the linkage oxygens, but it also relaxes more than the Mo(112) surface. The mismatch-induced strain is hence distributed between the siloxane surface and the α-quartz substrate, in contrast

to the Mo-substrate where only the siloxane surface is affected.

In summary, we have shown that the connectivity of the network found for the silica film on Mo(112) is not unique to this substrate, but appears to be common to a variety of hexagonal substrates. We suggest that it might exist on more substrates than currently known, provided that the lattice constant of the (quasi)hexagonal substrate is close to 5.25 Å and that the substrate offers oxygen adsorption sites in an approximately hexagonal arrangement. While the surface lattice of a Mo(112) c(2×2) structure is very close to that of the ideal siloxane surface, the linkage of the surface to the Mo rows introduces significant distortions. The siloxane surface can also be found on α-quartz when the surface is compressed by ∼8%. From our structural analysis, we conclude that the siloxane surface on Mo(112) found in the surface science experiments exhibits noticeable deviations from the ideal α-quartz surface although the chemical connectivity is identical. As we will see in the following, these differences induce changes for instance in the electronic structure and we expect that also the chemical properties are affected. We note also that the different relaxation behaviour of the two substrates may become important for the creation and reactivity of point defects in the film. While the α-quartz substrate readily supports relaxations around a point defect, this is not the case for Mo(112). Point defects in silica films on Mo(112) are indeed rare [106, 114].

The key factors for the substrate-induced structural changes identified here, namely the lattice constant and the interface constraints, can be used to discuss other thin film structures, too. We will take the the two-layer alumina film on NiAl(110) as an example. This film is easily obtained by exposing the clean metal surface to oxygen at elevated temperatures [98]. The self-limited oxidation results in a well-defined film that has been intensively studied over the last 15 years [15, 98, 115–117]. Only very recently, however, its complex structure could be finally solved by combining DFT calculations and STM investigations [15]. The film has a non-stoichiometric $Al_{10}O_{13}$ composition and exhibits Al atoms at the surface surrounded by three or four O atoms. These motifs have been interpreted as tetrahedral and truncated octahedral configurations. Kresse *et al.* have shown that the structure of the bottom (Al) layer is dictated by the preferential adsorption sites of the aluminium atoms on the NiAl(110) surface, i.e. by the interface to the substrate [15]. The substrate lattice also plays a considerable role for this film. The NiAl(110) surface lattice does not match with bulk alumina polymorphs. A comparison of the alumina bulk polymorphs reveals that changes in the lattice constant are always linked to changes in the coordination of the aluminium atoms. The varying coordination of the aluminium atoms found in the Al_2O_3/NiAl(110) film can thus be seen as a way of adapting the film to

the lattice constant of the substrate.[7] Both for silica and alumina, however, the interplay between the interface structure and the lattice relaxation stabilises structures of a particular thickness that do not correspond to a piece of the bulk material.

An example where the bulk structure is maintained and the thickness of the film can be varied is MgO on Mo(100) [19]. This film easily grows bulk-like despite a lattice mismatch of ∼5% because none of the dominant lattice relaxation mechanisms enforce deviations from the rocksalt structure. A complex interface structure does not develop because the flat MgO(100) surface matches reasonably with the Mo(100) substrate.

We conclude that crystalline oxide films with a bulk-like structure can only be grown on substrates where the surface lattice constant and the surface structure are compatible with the bulk material. How deviations of the ideal parameters are accomodated by the film then depends on the structural chemistry of the oxide. Silica and alumina, which have a very rich structural variety, will require very well tuned substrate properties to stabilise the bulk structures, whereas other oxides tolerate considerable deviations.

4.3.2 Electronic structure

We will now come back to the siloxane surface and compare the electronic structure of the siloxane surface on the Mo(112) substrate, i.e. the film found in experiment, and the α-quartz (0001) surface, which represents a perfect, dry silica surface. For the comparison of the different systems, we use the vacuum energy as a common energy zero.[8] Two important questions will guide us through the comparison: the more fundamental aspect if and how the hybridisation between the oxide surface and a metal substrate will affect the insulating character of the oxide surface, and the more case-specific question of how the changes in the atomic structure modify the features visible in the electronic structure. We will focus on the DFT-LDA electronic density of states (DOS) for this purpose. To compare to UPS or MIES experiments, the LDA band energies should be corrected for self-interaction and quasiparticle effects (e.g. with G_0W_0), and method-specific transition amplitudes should be taken into account. We will estimate the influence of these corrections when we discuss the connection to the experiments in Section 4.3.3.

[7] We note that the film is commensurate only along one direction (row-matching), while the incommensurate lattice along the other one introduces line defects.

[8] Alternative alignment strategies such as aligning the top of the valence band, or localised core states, yields similar results.

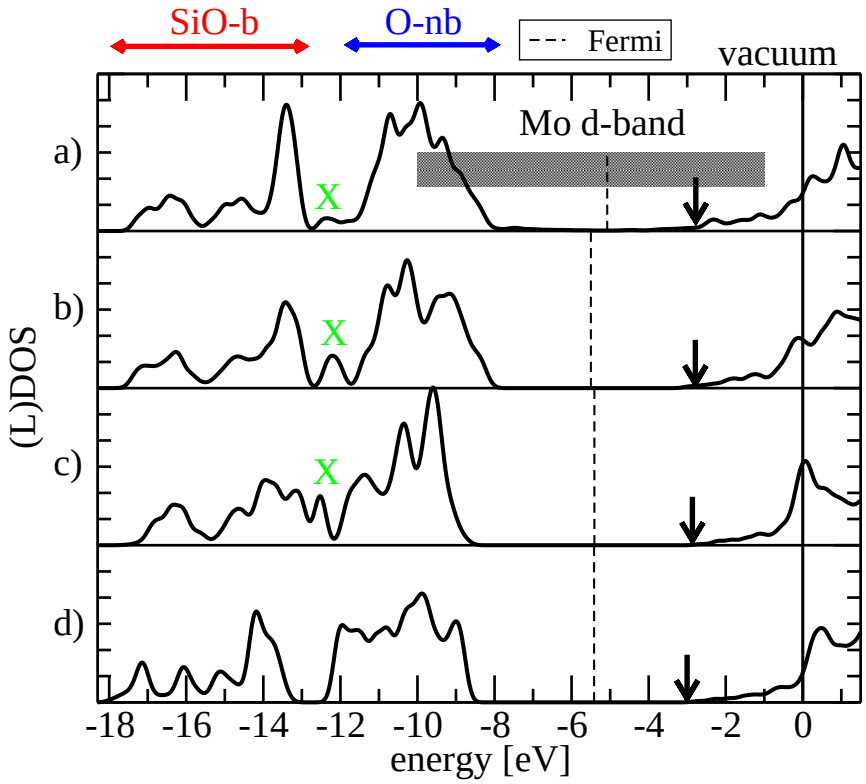

Figure 4.9: Surface LDOS for a) the silica film on Mo(112), b) the same, but the Mo atoms replaced by quartz (cf. text), and c) a relaxed α-quartz surface. d) Total DOS of bulk α-quartz. The X indicates the O-3mr feature between the SiO-b and O-nb subbands (cf. text). The bottom of the (surface) conduction band is marked by an arrow.

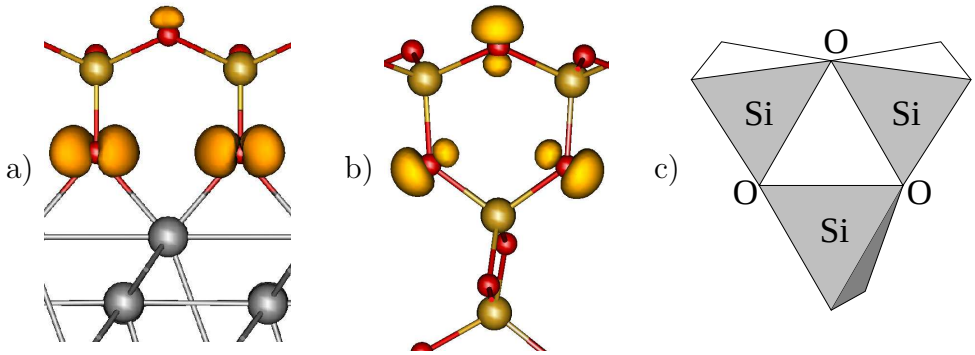

Figure 4.10: Isodensity surface for the partial density from the O-3mr peak on a) the Mo(112) and b) α-quartz substrates. c) Schematic representation of the 3-membered ring on α-quartz.

The surface LDOS (see Sec. C.2) for the siloxane surface on Mo(112) and quartz is presented in Fig. 4.9 a) and c). It can be understood on the basis of the α-quartz bulk bands, and we therefore include the total DOS of α-quartz as a reference. Surprisingly, the band edges at the surface agree with those of α-quartz to within 0.5 eV for both substrates. There are no surface states in the large band gap. The Mo metal states, which energetically lie within the surface band gap, play no important role at the surface. This indicates that the electronic structure of the defect-free surface and the substrate are essentially decoupled. The overall wide-gap insulating character of the siloxane surface resembles that of any other tetrahedral silica polymorph, independent of the substrate. However, an additional state (marked by X in Fig. 4.9) appears for the siloxane surface between the SiO-b and O-nb subbands. It is connected to the presence of almost planar "three-membered rings"[9] formed by two [SiO_4] units of the surface which are linked to the same substrate atom (Mo or Si). The state is composed of oxygen p-like orbitals (cf. Fig. 4.10) within the plane of the three-membered ring and will be denoted O-3mr in the following. It is thus not specific to the siloxane surface, but to a common motif of the interface to the Mo(112) and α-quartz substrates.

The peak structure in the valence region of the surface DOS, however, exhibits clear differences for the two substrates and deviates also from the DOS of bulk α-quartz. On Mo(112), there is a sharp feature at the top of the SiO-b subband, while the O-nb subband is relatively unstructured with three peaks and a broad flank. The tail of the unoccupied states shows

[9]The terminology in silica structures [112] refers to the number of [SiO_4] units in ring structures, not the number of atoms; cf. Fig. 4.10 c).

(small) resonances with the Mo states. On quartz, on the other hand, the O-nb region shows three strong features, whereas the top of the SiO-b band is less peaked than for Mo. The question now is whether these differences are related to the electronic structure of the substrate and/or the interface (the "chemical" influence) and what role the different atomic structure plays (the "structural" influence).

In order to disentangle the changes due to structural variations from other factors such as the chemical differences of the two interfaces, we have replaced the Mo(112) substrate by quartz (4 bulk-like layers + a siloxane surface). These additional atoms were fully relaxed while the original surface structure including the bridge oxygen atoms was kept fixed. The resulting surface DOS is shown in Fig. 4.9b. The differences between spectrum a) and b) in Fig. 4.9 thus reflect the chemical influence when the substrate is changed. The most important changes occur in the centre of the O-nb region and can be traced to the shifts in the mixed surface-interface states. Most of the spectrum, however, remains unaffected. The influence of the structure can be seen by comparing spectrum b) and c). When the lateral lattice is compressed to match α-quartz and the surface structure is fully relaxed, the SiO-b peak splits into two peaks and partially merges with the O-3mr feature at –12.5 eV. The O-nb region becomes more clearly structured and the band edges become steeper since the non-equivalence of the surface oxygens is reduced. We conclude from this that the changes in the local atomic structure induced by the substrate have a stronger influence on the shape of the electronic structure than the hybridisation with the substrate states.

Our findings can be summarised as follows: the global electronic structure of the siloxane surface is comparable to that of other tetrahedral silica polymorphs. It maintains a very ionic band structure with a large band gap. The band edges agree well with those of bulk α-quartz. A metallic substrate below the surface does not significantly alter the fundamental, strongly ionic characteristics of the electronic DOS. However, the substrate-induced variations in the atomic structure strongly modify the peak structure within the bands.

Before we address the implications of this for model catalysts and the surface science approach, we will first make a connection to available spectroscopic data.

4.3.3 Comparison to UPS and MIES experiments

The surface electronic structure of the siloxane surface has been characterised experimentally with UPS and MIES [17, 106]. The spectra show significant

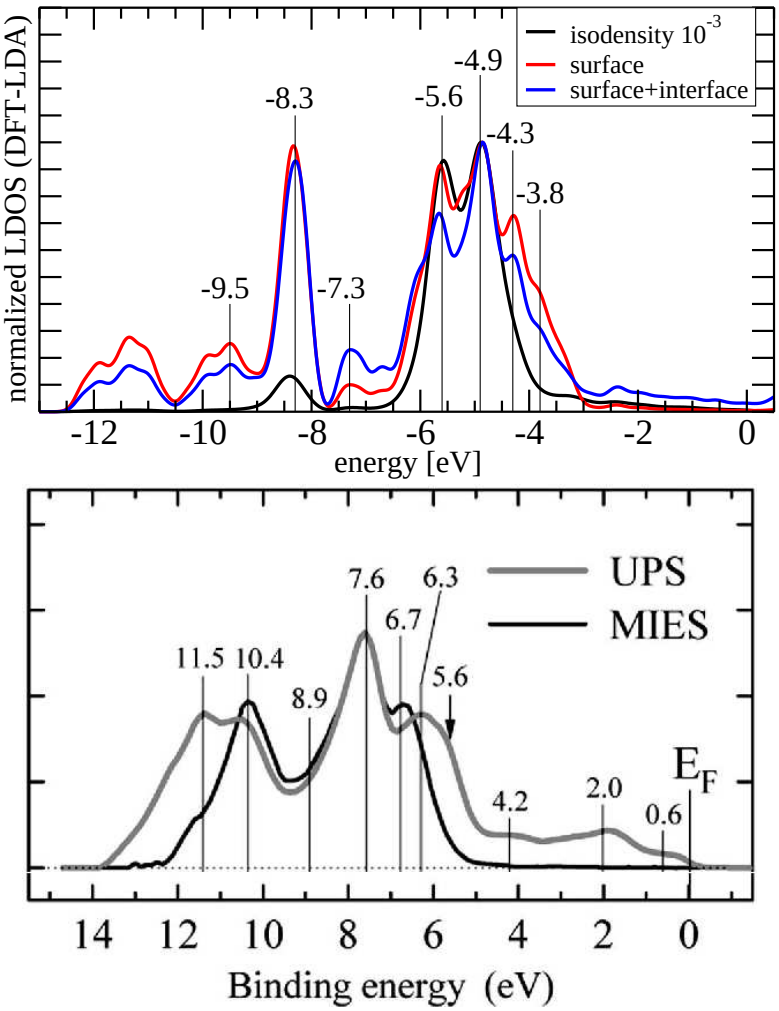

Figure 4.11: Top: Comparison of the local DOS in the LDA for different regions of the siloxane surface on Mo(112), see text. The spectra are normalised to the same maximum peak height. The (substrate) Fermi energy here defines the energy zero, i.e. the spectrum is shifted by 5.1 eV with respect to the vacuum-aligned spectra of Fig. 4.9. Bottom: Experimental spectra, taken from Fig. 4c) in [17].

differences due to the surface sensitivity of the two methods. In UPS, the electrons are excited by light which penetrates deep into the sample. In MIES, optically excited He atoms are shot at the surface which then emits electrons. While the probing depth of UPS is determined by the inelastic scattering of the emitted photoelectrons in the sample with typical mean-free paths in the 1-10 nm range, the MIES signal is believed to result mainly from Auger deexcitation of the incident helium atoms when electrons from the surface tunnel into the empty He 1*s* state [118]. Since the helium atoms never enter the surface in this case, the MIE spectrum is highly sensitive to the electronic structure of the surface, in particular to the tails of the electronic states at the surface. We have simulated this sensitivity be evaluating the DOS at an isodensity surface at low electron densities (10^{-3} e bohr^{-3}). In Fig. 4.11 we compare such an isodensity LDOS with the LDOS for two regions that may correspond to the surface sensitivity of the UP spectra, namely the topmost layer and the first two layers. We display both regions to demonstrate that the major differences occur between the isodensity LDOS and the surface-layer LDOS and not – as suggested in the original interpretation of the experiment [17] – between different oxygen layers.

The experimental MIE spectrum is considerably narrower than the UP spectrum, which was explained by the presence of an interface state at the top of the O-nb band [17]. The theoretical counterparts, i.e. the isodensity LDOS and the surface-region LDOS, reproduce the smaller band width, but suggests a different mechanism for the narrowing: the state at the top of the valence band that is visible only in UPS can be identified with a non-bonding *p*-orbital at the inter-row oxygen atom, oriented parallel to the surface plane (not shown). It is shadowed by the out-of-plane oxygen orbital at the same atom which extends further out into the vacuum and will thus be preferentially probed by the approaching He atom. At other surface atoms, the differently oriented orbitals cannot be associated with specific peaks in the spectrum. However, while the width of the spectra in the different techniques agrees well with our LDOS plots, the spectral intensities of the experimental spectra as well as the absolute position are not well reproduced by this simplified approach. In particular, the intensity at higher binding energies in the SiO-b region is significantly underestimated. Computing the spectral intensities, which depend on the state-specific transition amplitudes for each spectroscopic method, is outside the focus of this work. We therefore compare only the peak positions of the spectrum with experiment (cf. Tab. 4.2).

Since quasiparticle corrections are neglected in the computation of the DOS at the level of DFT-LDA and also due to inherent deficiencies of the LDA (self-interaction), the energetic position of the silica features with re-

		Si-O	O-3mr	O-nb			
UPS[a]	–11.5	–10.6	–	–7.6	–	–6.3	–5.6[c]
MIES[a]	–11.6[c]	–10.4	–	–7.6	–6.7	–	–
DFT-LDA[b]	–9.5	–8.3	–7.3	–5.6	–4.9	–4.3	–3.8[c]

[a] From Fig. 4c) in Wendt *et al.* [17]; [b] this work; [c] shoulder

Table 4.2: Peak positions relative to the Fermi level for the electronic surface DOS of the siloxane surface on Mo(112) in comparison with experiment. The theoretical data is not corrected for the estimated quasiparticle shift of 2 eV (see text).

spect to the Fermi energy is not well described. A scissor shift for the silica surface states can be estimated from bulk silica when possible local-structure, finite-size, surface, interface, and Fermi alignment effects are ignored. Using this crude approximation, we estimate that the computed position of the silica features in the valence region is too high by ∼2 eV, half of the quasiparticle corrections for the band gap of bulk silica[10]. Taking into account a quasiparticle shift of 2 eV, a good agreement with experiment for the silica film on Mo(112) is obtained. This agreement warrants the assignment of the peaks made in this section. It is interesting to note that Wendt *et al.* have interpreted these spectra as supportive evidence for their isolated SiO_4 cluster model [16], whereas we find that the electronic spectra are consistent with the siloxane surface model. It must be emphasised that the agreement between theory and experiment includes the features that were predicted to differ between the Mo(112) and the α-quartz substrates. We consider this strong evidence that the experimental spectra indeed reflect film-specific features rather than generic α-quartz features as claimed e.g. in [106]. The comparison to the DFT-LDA LDOS can help to understand the origin of the experimental signals, but to improve the agreement between theory and experiment regarding the absolute position and the spectral intensity, G_0W_0 should be applied to obtain a better quasiparticle band structure and also transition probabilities should be included.

[10] Chang *et al.* [119] report a quasiparticle correction for α-quartz of 4.5 eV, whereas our own G_0W_0 calculation give 3.4 eV. Ramos *et al.* [120] obtain corrections for β-cristobalite of 4.3–4.8 eV including a 0.2–0.3 eV overestimation due to certain approximations made.

4.3.4 How well do supported monolayer films model realistic surfaces?

As we have seen in this Section, a supported silica film of one monolayer thickness develops a structure that is directly influenced by the substrate. The ionic bonding within the film is not altered fundamentally compared to the situation in the bulk, but applying the same principles that govern the structure in bulk materials leads to a different result for thin films. For oxide films that develop a "chemical" interface to the substrate, i.e. which are linked to it by chemical bonds, the lattice is no longer determined by the oxide material itself, but by the respective substrate. The film seeks to maintain the local coordination of its ions wherever possible. A different lattice can therefore only be achieved by

1. compressing or stretching inter-ionic distances by small amounts,
2. distorting coordination shells,
3. introducing defects, or
4. developing new arrangements of the ions.

These effects can be recognised in the experimentally grown films. The first two points on the list become increasingly costly when the film becomes thicker. As suggested in point 3 of our list, thicker films grow often defective or even completely amorphous. New regular arrangements, on the other hand, can often only be stabilised as ultrathin films on a substrate. The required charge neutrality may involve the metallic substrate or the interface. Therefore, deviations from the bulk stoichiometry become possible such as the Si_2O_5 stoichiometry of the silica film on Mo(112), or also the $Al_{10}O_{13}$ stochiometry [15] of the thin alumina film on NiAl(110). Moreover, the different bonding situation at the interface and the surface already induces different local structures. We can consider these as alternative building blocks from which an ultrathin film structure is built. This may often lead to unique structures that are specific to one particular substrate and one particular thickness. However, even in the fortunate situation where the film structure is closely related to a bulk surface like the silica film on Mo(112), the local bonding arrangement is altered by the substrate.

While these changes play no important role for the ionic character of the chemical bonds, other properties may be more sensitive. We have seen in Section 4.3.2 that the peaks in the electronic DOS are strongly affected by the structure of the thin film. This has important consequences for defects created in the film. Since active defects in the band gap derive from bands

of the perfect material, the shifts observed for these bands should translate to similar shifts in the derived defect states. In addition, the existence of a Fermi level in the metal substrate may modify the charge state of the defects when electrons tunnel from or to these states [121]. We note that defects are very important for the chemical properties of the film. Since the perfect materials are chemically quite inert, the chemical reactivity of real materials is determined by the defects in the film. Our observations for the influence of the substrate on the electronic properties therefore suggests that also the chemical reactivity of supported monolayer films is modified by the substrate.

In summary, we find that oxide films that are only a few monolayers thick are strongly influenced by the substrate. They will in general not be representative for a bulk material or its surfaces. The changes in the local atomic structure, which are induced by the lattice constant and the interface to the substrate, play a crucial role: they induce further changes e.g. in the electronic structure and the chemical properties. The question now is if the comparability to the bulk can be improved by growing thicker films. We will therefore consider next the possibility to create films that do have bulk properties. We focus on one key aspect, namely the thickness.

4.4 Thickness dependence in freestanding films

We now address the surface science approach from a different angle and seek to establish a connection between ultrathin films and thick slab models for the surface of a bulk material. In order to see if ultrathin films can in principle have the same properties as the bulk oxide we eliminate the influence of the substrate by considering free-standing films (cf. step 2 in Fig. 4.1). By varying the film thickness we can tune our system between the two limits: ultrathin films and bulk surfaces. We have chosen three characteristic wide-gap oxides for these investigations: silica, alumina, and hafnia. The orientation of the films is chosen such that their surfaces correspond to the most stable, simple surface of the respective bulk material. We focus mainly on symmetric, stoichiometric films.[11] The thickness of the films is increased until an essentially bulk-like behaviour establishes. These thick films then correspond to the slab systems commonly employed in theory to model surfaces, i.e. we arrive at the situation that is sought in surface science experiments.

[11] For silica, also non-stoichiometric terminations were considered, but were found to be far less stable, see Sec. C.1.

4.4.1 α-Quartz

As in the previous section, we will focus our discussion on the development of the atomic structure first before we investigate the electronic structure for the most stable films obtained. For silica, several stoichiometric and non-stoichiometric terminations have been considered, see Appendix C.1 for details. In summary, quartz slabs with various surface terminations were constructed and their geometries were optimised. At all thicknesses, stoichiometric slabs with fully saturated bonds were found to be most stable. To achieve saturation, the two outermost quartz layers merge into one to form a siloxane surface or – in the smallest case – a similar structure. We will discuss here only the most stable structures, containing two to ten formula units (SiO_2) per (1×1) surface unit cell. Films with more than five formula units, i.e. Si_6O_{12} to $Si_{10}O_{20}$, are best characterised as α-quartz-like layers sandwiched between two siloxane surfaces. They correspond to two-sided[12] slab models of the (0001) surface of α-quartz. Thinner films deviate from this pattern in one way or another and we will briefly describe them one by one. The Si_5O_{10} structure contains only one intermediate layer between the siloxane surfaces and is highly strained. To saturate the bonds, the central Si atom must bind to two $[SiO_4]$ units of the upper surface and to two of the lower surface. A tetrahedral conformation at this atom would require a relative orientation of the two surfaces of 90°, but the three-fold symmetry of the ideal surface is only compatible with steps of 120°. The result (cf. Fig. 4.12a) is a distorted structure in which the $[SiO_4]$ tetrahedra at the surface are tilted by 28.5°. The most stable structure found for Si_4O_8 is the siloxane pure-surface film already discussed in Section 4.3 (cf. Fig.4.6), in which two siloxane surfaces are directly linked together. We exclude the Si_3O_6 case from the discussion here since it inevitably exhibits dangling bonds at variance with all other films. The most stable structure for Si_2O_4 turns out to be a single-layer two-dimensional network with hexagonal rings, where two oxygen atoms lie in the Si plane, while the two others form an out-of-plane two-membered silica ring (cf. Fig. 4.12b), a motif known from other silica surfaces [14, 122].

In the previous section we have already presented the siloxane surface as the most stable reconstruction of the α-quartz (0001) surface. A remarkable point of this surface reconstruction is that it restores the $[SiO_4]$ units with fully saturated bonds at the expense of their long-range order and the Si-O-Si

[12] The two surfaces are equivalent, but the slabs are not symmetric. The only non-trivial symmetry (i.e. which is not a pure translation) of bulk α-quartz is a screw axis along (0001), which is necessarily lost when then translational symmetry along (0001) is broken.

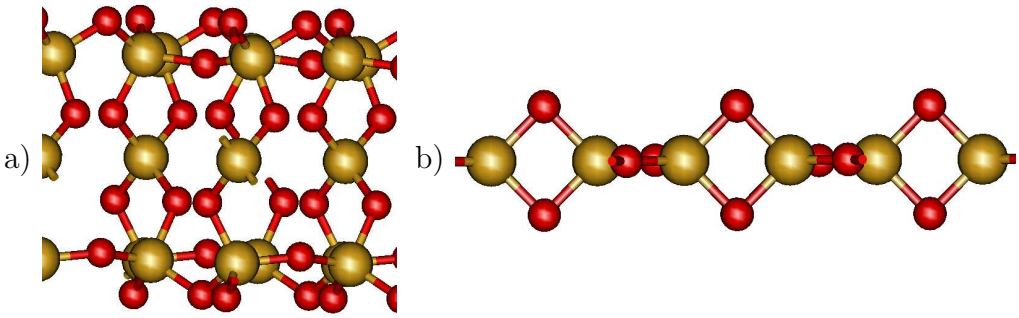

Figure 4.12: Side-view of reconstructed films: a) Si_5O_{10} and b) Si_2O_4.

angles. In other words, the long-range structure is strongly modified to reduce or even remove the perturbations in the local atomic structure. We find the same trend for the ultrathin films. The saturation of the dangling bonds appears to be a very strong driving force for the reconstructions observed. It is supported by the flexibility of the Si-O-Si angles, i.e. the connections of the $[SiO_4]$ units in the silica network. The strain induced by the reconstructions is distributed in the network. Correspondingly, we find a strong variation of the Si-O-Si angles with the film thickness.

What does this imply for the use of silica films in the surface science approach? First, we note that the reconstructions required to saturate dangling bonds drastically modify the atomic structure at small thicknesses. A thickness of six formula units is necessary before a bulk-like central part covered by a siloxane surface forms. We note that in real systems the presence of water will offer an alternative to the reconstructions observed here, namely the saturation by hydroxyl groups. We therefore expect that the tendency to form hydroxyl groups will strongly depend on the thickness. Second, the strain induced by the reconstructions is distributed over the network. This has important consequences for the geometrical relaxation around defects and the strain induced by it. Only thicker films can include α-quartz-like layers, which in general are very flexible, and can thus reduce strain at the expense of long-range relaxations. In thin films, distortions will be more localised leading to higher strain. Last, we have seen that the reconstructions at the surface include the two outermost layers. This indicates that reactions at the surface may involve one or more subsurface layers, and these are not present or behave differently in ultrathin films.

We now come to the discussion of the electronic structure for these films. The total DOS for the different reconstructed slabs is displayed in Fig. 4.13. For two or more quartz-like layers, i.e. from Si_6O_{12} on, the changes in the DOS become rather small and reflect mainly the varying relative contribu-

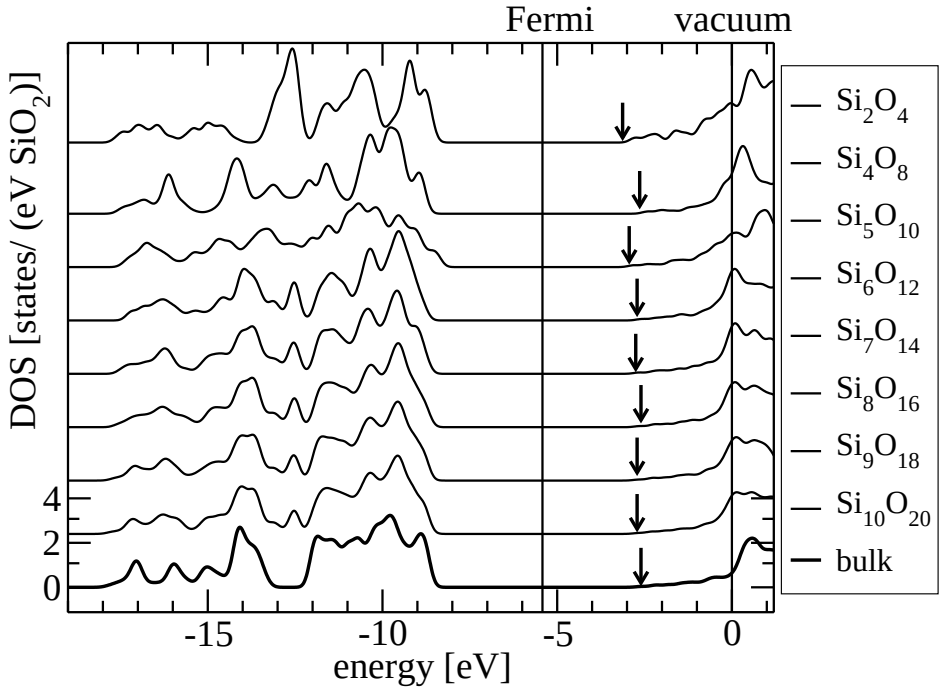

Figure 4.13: Thickness dependence of the DOS for stoichiometric thin silica slabs. The bottom of the conduction band is marked by an arrow.

tion of the thickness-independent surface features[13] to the total DOS. The thinner films exhibit stronger differences, which we attribute to the structural variations described above. In all these ultrathin films, a gap between the Si-O bonding and the O non-bonding does not exist, in contrast to all 4:2-coordinated silica bulk polymorphs.[14] Surprisingly, the band edges and band widths are affected very little by the thickness variation, even for the thinnest films. While this is to be expected for localised states[15], notably the O-nb states, the insensitivity of the lowest conduction band which is a highly delocalised state in the bulk seems contradictory. For such a state, one could expect similar confinement effects as they are observed in ultrathin semiconductor and metal films [123, 124]. We attribute the absence of such an effect to a surface resonance that traces the edge of the projected bulk bands. It couples to the bulk bands at $k_z \approx 0$ as is visible from the flat envelope function along the z-direction. In Fig. 4.14, we demonstrate this for the conduction band minimum. Since $k_z = 0$ implies a constant phase, the coupling between the surface resonance and a $k_z = 0$ bulk band is independent of the film thickness, giving rise to the thickness-independent feature in the band structure. This highlights that the magnitude of possible confinement effects cannot be estimated from the bulk bands alone, but also the scattering properties at the surface play a decisive role.

We conclude that ultrathin silica films will usually not resemble any bulk-like structure even if the lattice constant is chosen in accordance to the bulk. To saturate the dangling bonds, strong relaxations occur that have a drastic effect on the shape of the electronic structure. Even the characteristic gap between the SiO-b and O-nb regions of the spectrum disappears. The band edges, however, are almost independent of the thickness. This demonstrates that the band gap is no useful parameter to assess the changes in the electronic structure for ultrathin silica films. Although the perfect films discussed here are expected to be chemically inert due to the large band gap, realistic, defective films will differ in their chemical properties because the changes observed within the perfect bands will translate to corresponding changes in the defect states derived from them. However, we note that relatively few bulk-like layers in the centre of the slab (two in the case of α-quartz) are

[13] The surface LDOS presented in Fig. 4.9 c) gives an impression of these features.

[14] Other than for the siloxane surface, no particular structure motif can be made responsible for this observation.

[15] We note that "localised state" refers here mainly to the character of the atomic orbitals from which the state derives, showing only little inter-atomic overlap. The Kohn-Sham eigenstates, however, are not localised in one part of the slab, but typically extend over the slab. The envelope function typically shows a sine-like, confined shape, but this has no dominant influence on the energy of this state.

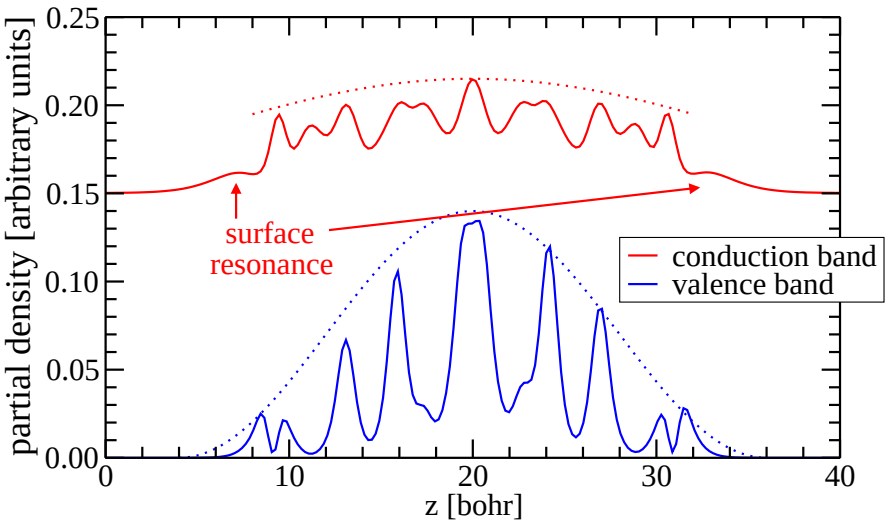

Figure 4.14: Partial electron density profiles (normalised to 1) for the valence band maximum and the conduction band minimum of the Si_8O_{16} slab. While the envelope of the valence state shows a typical confined shape, the conduction band is very flat due to its coupling with a surface resonance.

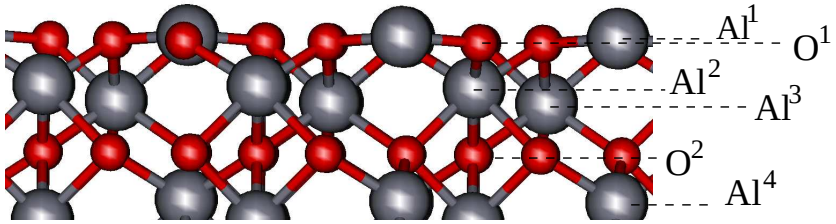

Figure 4.15: Side view of the (0001) surface of α-Al_2O_3. The letters denote the vertical position of the topmost Al and O layers.

sufficient to approach the bulk properties.

4.4.2 α-Alumina

As a second example we consider alumina, which is another important material for heterogeneous catalysts. Thin alumina films have been grown on a wide variety of substrates [11], but the well-ordered epitaxial films are generally found to exhibit large and complex unit cells. The detailed atomic structure has been recently solved for the 5 Å thick film on NiAl(110) [15], but it is often not known for other substrates. We therefore do not try to approach one particular film, but restrict ourselves to the most stable bulk polymorph, α-alumina. We have chosen the 1×1 (0001) surface with an

	Al_4O_6	Al_6O_9	Al_8O_{12}	$Al_{10}O_{15}$	$Al_{12}O_{18}$
Δ (Al^1-O^1) [%]	-62.4	-96.3	-86.9	-85.1	-85.7
Δ (O^1-Al^2) [%]	+28.3	+3.5	+2.5	+4.2	+4.0
Δ (Al^2-Al^3) [%]	-100.0	-52.7	-40.3	-44.6	-44.4

Table 4.3: Thickness dependence of the inter-layer relaxation Δ between the first layers at the surface of α-alumina slabs.

Al-O_3-Al-termination, which is the most stable termination in the absence of hydrogen [125]. Stoichiometric slabs of varying thickness can be constructed by adding Al-O_3-Al layers. We investigated slabs with a thickness of up to six of these triple layers, i.e. $Al_{12}O_{18}$.

The topmost aluminium atom at the (0001) surface shows a very strong inward relaxation, thereby becoming almost coplanar with the oxygen layer (cf. Fig. 4.15). This is easily explained: compared to the bulk, the surface aluminium ion has lost three of its six oxygen neighbours. The ideal local arrangement for the reduced coordination would be trigonal. To approach this configuration, the Al ion relaxes strongly inward, thereby pushing the oxygen ions aside. These relaxations at the surfaces then induce further changes in the deeper layers. Interestingly, we find in our DFT-LDA calculations that the magnitude of the surface relaxation depends on the thickness of the slab. To monitor these changes, we focus on the relative change Δ(L-L') in the separation between the layers L and L'. The layers are denoted by the atom type, i.e. Al or O, and are then simply counted by increasing depth, i.e. the first layers are Al^1-O^2-Al^2-Al^3-O^2-Al^4-... as indicated in Fig. 4.15. The computed interlayer separations at the surface are summarised in Tab. 4.3 and demonstrate that there is a delicate, non-monotoneous balance of the relaxations in the different layers.

These changes in the atomic structure are very important for the adsorption of atoms or small molecules. On ionic surfaces with low-coordinated atoms, electric fields play an important role not only for the energetics of the adsorption [126, 127], but they may also activate or deactivate bonds in subsequent reactions [128]. The strength of these fields strongly depends on the local geometry. We therefore have to expect a considerable influence of the film thickness on the adsorption properties when only a few monolayers of the oxide are present. For the α-alumina slabs a thickness of four oxygen layers ($\sim$10 Å) is required to obtain a surface relaxation close to that of a bulk substrate (cf. Tab. 4.3).

Are these variations in the relaxation also reflected in the electronic structure, and will they exert a similar influence on the shape of the electronic spectrum as we had observed for silica? The total DOS for the relaxed slabs,

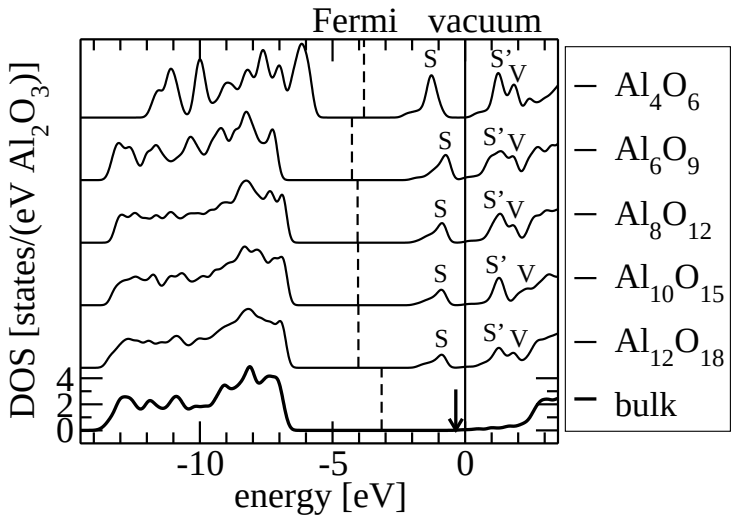

Figure 4.16: Thickness dependence of the DOS for stoichiometric thin α-alumina slabs in comparison to the bulk DOS. The vacuum energy defines the energy zero. The arrow marks the bottom of the conduction band in bulk alumina. S and S' denote the Al-derived surface states. V is a confined vacuum state, a meaningless artifact of the repeated-slab approach.

shown in Fig. 4.16 in comparison to bulk alumina, gives an answer to these questions. The most striking difference to the silica films is the appearance of a surface state in the band gap of the bulk material. It derives from the unoccupied aluminium states at the surface and overlaps energetically with the bottom of the O-3*s*-derived bulk conduction band. A second Al-derived surface feature is positioned energetically above the vacuum energy. The lower energy of the aluminium states at the surface relative to the bulk results from the reduction in the Madelung potential at the surface when going from a 6-fold to a 3-fold coordination [129].

We now turn our attention to the valence region. The DOS of the thinnest film differs dramatically from all others: the valence states are shifted by more than 1 eV relative to the conduction states and the vacuum level. A similar effect has been observed earlier for freestanding MgO films by Pacchioni *et al.* [91]. They concluded that the Madelung potential, which stabilises the ionic state, evolves only after a few monolayers. What can be observed for the Al_4O_6 film is a breakdown of the bulk ionicity, which reduces the energy separation of the anion and cation states. The thickness-dependent relaxation leads additionally to a variation of the surface dipole and hence the alignment of the DOS with respect to the vacuum energy. The calculated Fermi energy then varies strongly between the thinnest films because it coincides with the

centre of the band gap and thus reflects the gap changes from the Madelung effect as well as the changes in the surface dipole. The atomic structure in the central part of the thicker films, i.e. from Al_6O_9 on, corresponds to almost perfect corundum and we find an essentially bulk-like valence electronic structure for these films. Only the density of states of the thinnest film differs significantly from the bulk. The quick, almost sudden emergence of a bulk-like shape with increasing thickness differs from the trend observed for silica. We can relate this to the structural relaxation mechanism in the two materials. The local coordination of the oxygen atoms is very important for the valence electronic structure, which is dominated by the oxygen $2p$ orbitals. In silica, the structure relaxation affects mostly the oxygen atoms. The structural changes therefore visibly modify the electronic structure. In alumina, on the other hand, the deformation of the coordination shell of the aluminium ions is the dominant structural relaxation mechanism, which has no important influence on the O-$2p$-derived valence states.

The observed bulk-like behaviour for the films beyond Al_6O_9 is relevant for a second area of application of thin alumina films, namely its possible use in electronic devices. In field-effect transistors (cf. Fig. 1.3), from which the basic logic elements in integrated circuits are built, the gate electrode must be electrically insulated from the conducting channel that the gate electrode controls. This is achieved by a thin insulating film, the gate dielectric. The capacitance of the film must be low to reduce the switching currents, but the film must be thick enough to avoid leakage currents due to defects or – in particular for ultrathin films – due to tunneling. The dielectric constant (often denoted as κ in this context) should be as large as possible to increase the physical thickness of the insulating film. In addition, the band alignment between the semiconductor and the insulator must create large barriers for the tunneling currents. In silicon-based semiconductors, amorphous silica has been the material of choice for this purpose. The on-going miniaturisation of the electron devices and new semiconducting materials, however, requires alternative high-κ materials. Among others, alumina and hafnia (which we will discuss below) have been considered as a possible replacement. Our results indicate that the relevant macroscopic properties of bulk alumina are preserved down to thicknesses of about 10 Å. Only then, size-effects and a break-down of the bulk behaviour must be taken into account.

4.4.3 Cubic hafnia

We now turn to hafnia as the last example, which will complete our study of the thickness dependence. In contrast to alumina and silica, hafnia plays no important role for catalytic applications. However, it has attracted consid-

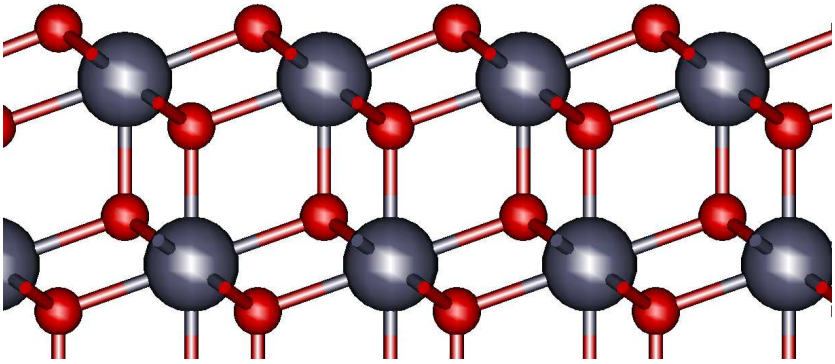

Figure 4.17: Side view of the (111) surface of cubic HfO_2.

erable interest for electronic devices due to its large dielectric constant [22]. We have therefore chosen to include this material in our investigations of the thickness dependence. In experiment, hafnia films are usually grown epitaxially on semiconductor substrates, in particular silicon. X-ray diffraction studies have indicated that these epitaxial films may consist of cubic hafnia [99, 100]. However, the structural characterisation at the atomic level is less detailed than for the alumina films.

Electrostatic considerations predict the (111) surface to be the most stable unreconstructed surface, and stoichiometric slabs can then be constructed by adding O-Hf-O layers. The (111) surface is very dense, i.e. only few ionic bonds are broken. The outermost oxygen atoms miss one of their four bulk neighbours, and the Hf ions only one out of eight. Correspondingly, the surface relaxations are much smaller than in alumina and show almost no dependence on the thickness. We can compare the situation to the (001) surface of rocksalt oxides such as MgO, that also show very small relaxations at the surface [129]. We can identify here a clear trend. The higher the coordination numbers in the bulk and the denser the surface termination, the smaller the relaxations at the surface and their sensitivity to the film thickness. This trend has been already visible in the comparison of the reconstructing, 4:2-coordinated silica to the more densely packed, 6:4-coordinated alumina, and continues to the 8:4-coordinated cubic hafnia.

We find a similar result for the electronic structure, cf. Fig. 4.18. From three (triple) layers on, i.e, Hf_3O_6, the DOS in the valence region is bulk-like. The thinnest film Hf_2O_4, which contains only undercoordinated Hf ions, shows again a different shape of the electron spectrum than the bulk which mainly reflects the surface electronic structure. We note that the trifold-coordinated oxygen atom introduce a state right at the top of the bulk valence band which is responsible for the steeper band edge of the thinnest films. In

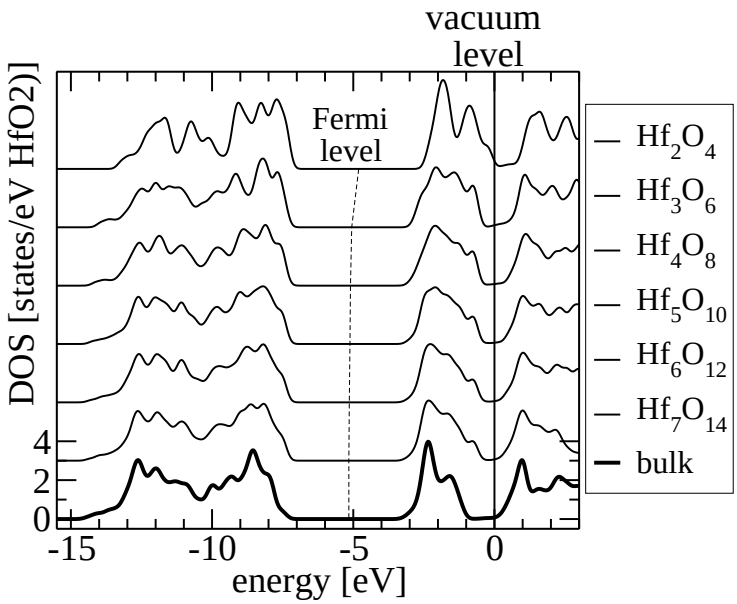

Figure 4.18: Thickness dependence of the DOS for stoichiometric cubic hafnia slabs in comparison to bulk HfO_2.

the conduction band, the Hf e_g states are shifted towards higher energies at the surface, i.e. the opposite direction than for the aluminium surface state in alumina. For hafnia, the change in the Madelung potential at the surface is apparently less important than the reduction of the crystal field splitting. Like for alumina, the evolution of the DOS of thicker films can be understood in terms of a simple mixture of bulk-like and surface-like features. When the thickness is increased, a bulk-like DOS appears quite suddenly above a minimum thickness of four oxygen layers. For both materials, we then find the atoms in the central part of the slabs in a bulk-like environment. We conclude that the macroscopic electronic properties of both alumina and hafnia are essentially identical to those of the bulk materials above $\sim$10 Å thickness. For thinner films, however, we find considerable changes.

4.5 Summary

In this Chapter, we have studied the atomic and electronic structure of epitaxial thin films of wide-gap oxides by means of density-functional theory. We have made contact to two important fields of application for oxide films, namely the "surface science approach" to study heterogeneous model catalysts and to electronic devices. We have shown that the structural and elec-

tronic properties of ML-thin oxide films systematically deviate from thicker films and bulk oxides. On the one hand, the substrate crucially influences and modifies the atomic structure. We have shown that the structural relaxations can be explained in terms of the same principles that govern the relaxation in the corresponding bulk structure(s), but the particular situation at the individual surface must be taken into account. We have identified the substrate lattice for commensurate thin films and the interface to the substrate as two key factors that determine the structural constraints for supported thin films, and demonstrated that these key factors can explain many of the structural trends observed for epitaxial oxide films grown on metals. We have then turned our attention to the role of the thickness of the film. Again, we find considerable differences between monolayer-thin films and the bulk materials even if we explicitly exclude any influence from a possible substrate. We have seen that the atomic structure sensitively depends on the thickness below a critical size. Close-packed structures and high coordination numbers in the bulk reduce the thickness sensitivity of the film properties. The largest changes are found for silica due to its high structural flexibility. While the band gaps and band widths are usually very close to the corresponding bulk values even at very small thicknesses, peaks in the electronic spectrum are very sensitive to the structural changes for monolayer-thin films. However, comparatively few bulk layers in the centre of the films are sufficient to obtain a bulk-like electronic structure and converged surface properties. This suggests that already films with a few more monolayers than the currently prevailing one- and two-ML films may be sufficient to improve the comparability to the surfaces of bulk materials. It must be emphasised that a larger total thickness of the film alone will not be sufficient to achieve this; it is decisive that bulk-like layers are present below the surface. A crucial point, however, is to find substrates that are compatible with the corresponding bulk structures not only in terms of the lattice constant, but also for a smooth interface to the bulk structure.

Before concluding this Chapter, we should briefly return to the outset. The original motivation for studying ultrathin epitaxial films in the context of heterogeneous catalysis was to learn more about the relevant microscopic properties of catalysts from simple model systems. We have then seen in this Chapter that epitaxial monolayer films are neither simple, nor are they representative models for the surfaces of the bulk oxides. However, even the ideal surface of a bulk oxide itself differs drastically from a real support material's surface and may lack decisive features. Of crucial importance is the influence of the gas phase. Under atmospheric pressure, the surface will be completely covered by adsorbates, in particular by hydroxyl groups created by the dissociation of water. Apart from defects, hydroxyl groups

are a second type of chemically reactive surface species, in particular for proton transfer reactions. Likewise, they can act as anchors for metal ions by exchanging the hydroxyl proton for the metal ion. The presence of water can also modify the thermodynamical stability as has been demonstrated for the α-alumina (0001) surface [125]. While the dry surface has a positive surface energy (in agreement with our freestanding films), the presence of hydrogen at the surface makes the surface energy negative.[16] We note that the density of hydroxyl groups on a crystalline film can differ substantially from that of a realistic surface under the same conditions: A film grown in the absence of water may not be very reactive when exposed to water afterwards [130], while a real surface is usually created in the presence of water and will most likely immediately incorporate it into the surface.

For the chemical reactivity of a surface under real conditions, point defects play an important role. Their stability and reactivity however depends crucially on the charge state, which is determined by the Fermi energy of the system. For film systems, the metal substrate defines the Fermi energy. In the absence of a metal, i.e. in real catalysts, the Fermi energy depends on the defects and dopants (the "dirt") and is thus influenced by the treatment of the sample. This implies that the substrate of the epitaxial films in the surface-science approach fixes a possibly important degree of freedom. In addition, the defect levels themselves may be modified by the structure of the epitaxial film as we have discussed in Sec. 4.3.4.

Bearing these restrictions in mind, the epitaxial films are invaluable for improving our understanding of heterogeneous catalysts and related surface phenomena. Experiments on thin epitaxial films allow us to take a much more detailed look at insulator surfaces than would otherwise be possible at the moment. Theory then offers a complementary view on the experimental observations and how they relate to the true systems of interest.

[16] Thermodynamically, the crystal should thus split into small particles with hydroxyl-covered surfaces. In practice, this reaction runs at negligible speed and α-alumina is very inert towards water [94].